Cell Reports

STING is an intrinsic checkpoint inhibitor that restrains the T_H17 cell pathogenic program

Graphical abstract

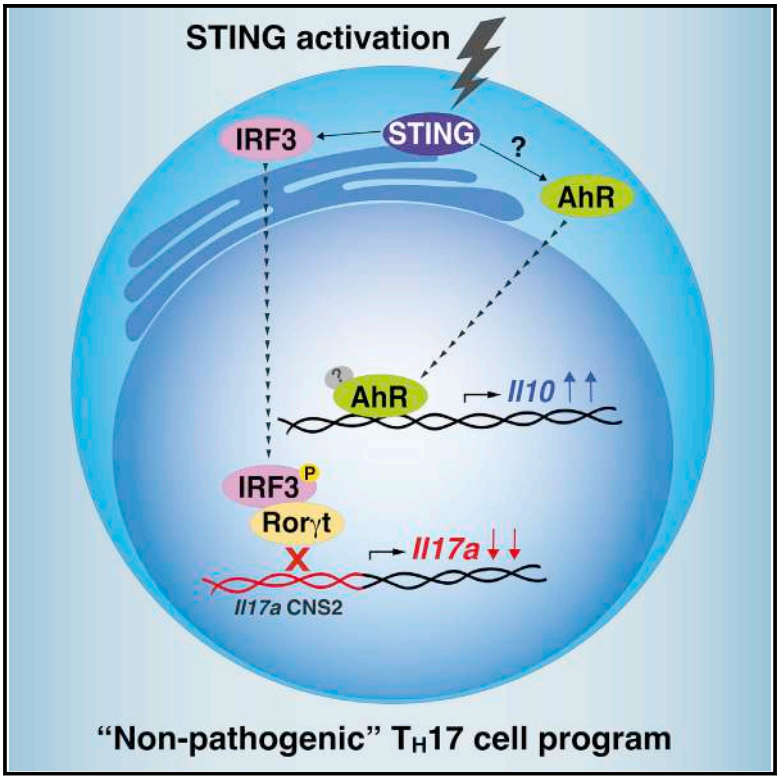

Highlights

- The expression of STING is inversely associated with T_H17 cell pathogenic state
- AhR signaling is involved in the STING-driven IL-10 expression in T_H17 cells
- STING activation impairs Rorγt binding to *Il17a* CNS2 enhancer region

Authors

Luis Eduardo Alves Damasceno, Guilherme Cesar Martelossi Cebinelli, Mariane Font Fernandes, ..., Thiago Mattar Cunha, Fernando Queiroz Cunha, José Carlos Alves-Filho

Correspondence

jcafilho@usp.br

In brief

T_H17 cells display a spectrum of pathogenic states depending on environmental and intrinsic cues. Damasceno et al. demonstrate that STING activation induces a non-pathogenic T_H17 profile. Mechanistically, STING impairs Rorγt-mediated *Il17a* transcription, thereby reducing IL-17A production. Besides that, STING activation promotes IL-10 expression through AhR signaling pathway.

Damasceno et al., 2022, Cell Reports *39*, 110838
May 24, 2022
https://doi.org/10.1016/j.celrep.2022.110838

CellPress

Cell Reports

CellPress
OPEN ACCESS

Report

STING is an intrinsic checkpoint inhibitor that restrains the T_H17 cell pathogenic program

Luis Eduardo Alves Damasceno,[1,2] Guilherme Cesar Martelossi Cebinelli,[1,2] Mariane Font Fernandes,[3] Daniele Carvalho Nascimento,[1,2] Gabriel Azevedo Públio,[1,2] Marco Aurélio Ramirez Vinolo,[3] Sergio Costa Oliveira,[4] Tim Sparwasser,[5] Thiago Mattar Cunha,[1,2] Fernando Queiroz Cunha,[1,2] and José Carlos Alves-Filho[1,2,6,*]

[1]Department of Pharmacology, Ribeirao Preto Medical School, University of Sao Paulo, Ribeirao Preto, SP 14049-900, Brazil
[2]Center for Research in Inflammatory Diseases, Ribeirao Preto Medical School, University of Sao Paulo, Ribeirao Preto, SP 14049-900, Brazil
[3]Laboratory of Immunoinflammation, Department of Genetics, Evolution, Microbiology, and Immunology, Institute of Biology, University of Campinas, Campinas, SP 13083-862, Brazil
[4]Department of Biochemistry and Immunology, Institute of Biological Sciences, Federal University of Minas Gerais, Belo Horizonte, MG 31270-901, Brazil
[5]Institute of Medical Microbiology and Hygiene, University Medical Center of the Johannes Gutenberg-University, Mainz 55131, Germany
[6]Lead contact
*Correspondence: jcafilho@usp.br
https://doi.org/10.1016/j.celrep.2022.110838

SUMMARY

External and intrinsic factors regulate the transcriptional profile of T helper 17 (T_H17) cells, thereby affecting their pathogenic potential and revealing their context-dependent plasticity. The stimulator of interferon genes (STING), a component of the intracellular DNA-sensing pathway, triggers immune responses but remains largely unexplored in T cells. Here, we describe an intrinsic role of STING in limiting the T_H17 cell pathogenic program. We demonstrate that non-pathogenic T_H17 cells express higher levels of STING than those activated under pathogenic conditions. Activation of STING induces interleukin-10 (IL-10) production in T_H17 cells, decreasing IL-17A and IL-23R expression in a type I interferon (IFN)-independent manner. Mechanistically, STING-induced IL-10 production partially requires aryl hydrocarbon receptor (AhR) signaling, while the decrease of IL-17A expression occurs due to a reduction of Rorγt transcriptional activity. Our findings reveal a regulatory function of STING in the T_H17 cell activation program, proposing it as a valuable target to limit T_H17-cell-mediated inflammation.

INTRODUCTION

T helper (T_H) cells are prone to undergo transcriptional, epigenetic, and post-translational modifications induced by environmental and intrinsic factors that affect their phenotype and function (Chang et al., 2014). T helper type 17 (T_H17) cells are implicated in the host immune response against pathogens, but they also mediate autoimmune inflammation, giving rise to the dual nature of "non-pathogenic" and "pathogenic" T_H17 cell populations and highlighting its complex context-dependent plasticity (Stockinger and Omenetti, 2017). For instance, T_H17 cells can transdifferentiate into interleukin-10 (IL-10)-producing T_H17 cells after reaching the inflammatory site (Gagliani et al., 2015). Therefore, understanding the molecular mechanisms involved in T_H17 cell plasticity might expand the perspectives for treating T_H17-mediated inflammatory diseases.

Recognition of microbial nucleic acids is a mechanism of the innate immune system to respond against pathogens (Tan et al., 2018). The adaptor protein stimulator of interferon genes (STING) links nucleic acid cytosolic sensing with immune cell effector functions (Motwani et al., 2019). STING is activated by microbial-derived cyclic dinucleotides or generated by sensors like cGAS following recognition of cytosolic double-stranded DNA (Burdette et al., 2011; Sun et al., 2013), but it can also directly bind to DNA (Abe et al., 2013). Once activated, STING induces the expression of type I interferon (IFN) via the TBK1-IRF3 signaling pathway, contributing to antiviral response (Ishikawa and Barber, 2008; Zhong et al., 2008). Although most studies reveal the importance of STING for antimicrobial immune responses, there is some evidence that it negatively regulates inflammation. For instance, colitis-bearing STING-deficient mice develop severe disease associated with higher levels of IL-17 in the colonic tissue and decreased IL-10 expression in lymph nodes (Canesso et al., 2018). Also, STING activation is involved in the production of IL-10 needed for intestinal immune homeostasis (Ahn et al., 2017). However, while the expression of STING in T cells is documented (Cerboni et al., 2017; Gulen et al., 2017; Larkin et al., 2017), its intrinsic role in T_H17 cells remains unclear.

Here, we unveil the role of STING as an intrinsic checkpoint inhibitor that restrains the T_H17 cell pathogenic program.

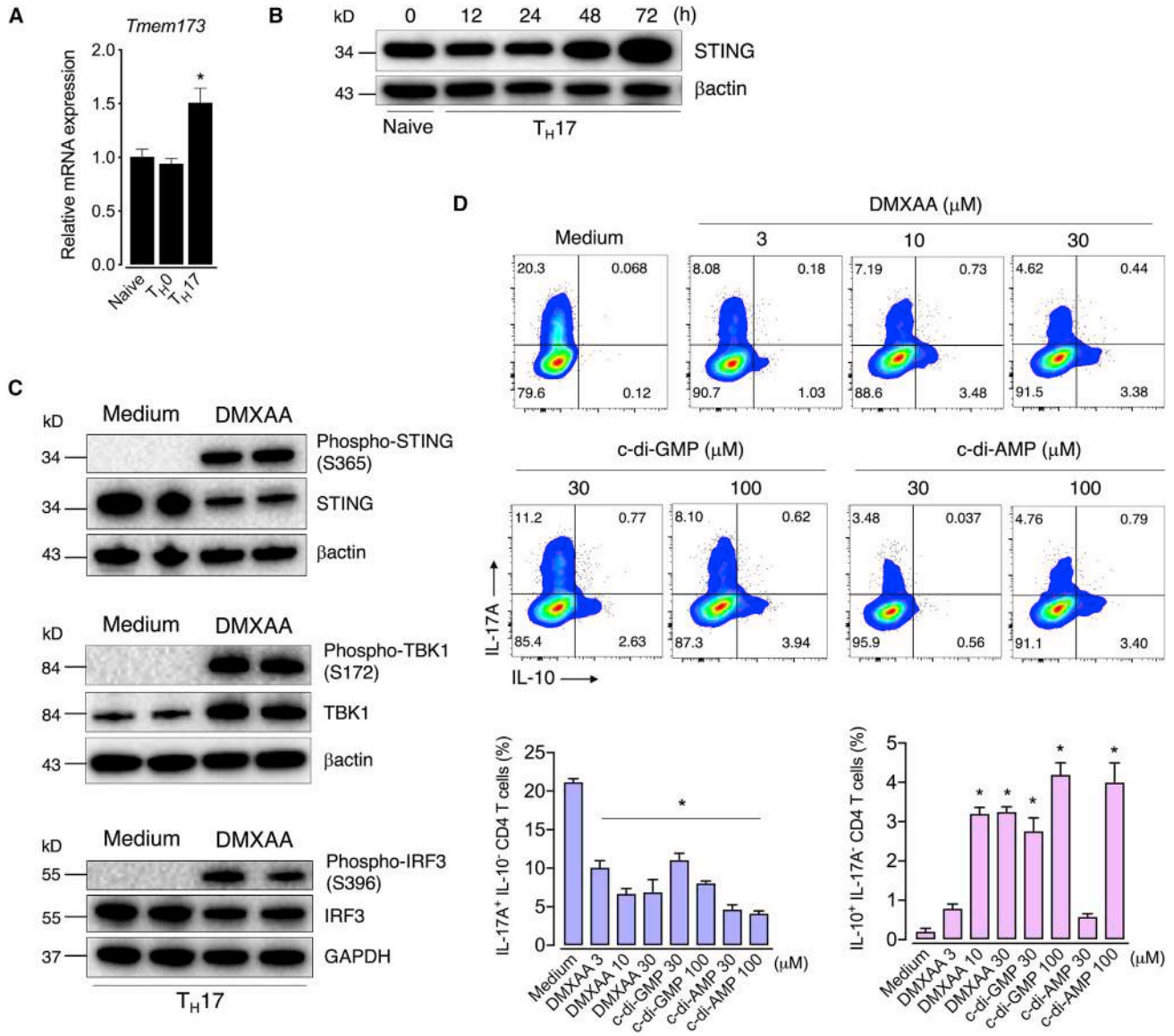

Figure 1. STING regulates effector cytokine profile in T_H17 cells

(A) *Tmem173* mRNA expression in naive or TCR-activated CD4 T (T_H0) and T_H17 cells at 48 h of culture. Fold change relative to naive cells (n = 3).

(B) Kinetics of STING protein expression in T_H17 cell during differentiation determined by immunoblot. β-actin was used as the loading control.

(C) Immunoblot analysis of STING downstream signaling components in control (medium) and DMXAA-treated (10 μM) T_H17 cells collected at 72 h of culture. β-actin or GAPDH was used as the loading control.

(D) Flow-cytometric analysis of IL-10 and IL-17A expression in T_H17 cells differentiated with increasing concentrations of DMXAA, c-di-AMP, or c-di-GMP for 72 h (n = 3–5).

Data are representative of at least two independent experiments and are shown as mean ± SEM. *p < 0.05 determined by one-way ANOVA followed by Tukey's post hoc test compared with naive (A) or control (D) groups.

RESULTS AND DISCUSSION

STING activation switches T_H17 effector cytokine profile

To determine the role of STING in T_H17 cells, we initially analyzed its expression profile in T cells. We found that both naive and T cell receptor (TCR)-activated CD4 T cells (T_H0) express STING mRNA levels (encoded by the *Tmem173* gene), which were higher in T_H17 cells generated *in vitro* (Figure 1A). Protein levels of STING also increased over the time of T_H17 cell differentiation (Figure 1B). To determine the role of STING in T_H17 cells, we differentiated T_H17 cells with IL-6 and transforming growth factor beta (TGF-β) in the presence of DMXAA, a murine STING agonist (Prantner et al., 2012). We also used cyclic dinucleotides c-di-AMP and c-di-GMP, which are naturally signaling molecules in bacteria that activate STING (Burdette et al., 2011). Upon activation, STING recruits

TBK1 that phosphorylates both STING and IRF3, leading to type I IFN production (Liu et al., 2015; Tanaka and Chen, 2012; Zhang et al., 2019). Accordingly, we observed that all these STING signaling cascade components were activated in T_H17 cells treated with DMXAA (Figure 1C). Unexpectedly, the addition of DMXAA, c-di-AMP, or c-di-GMP to the T_H17 cell cultures reduced the production of IL-17A while increasing the frequency of the IL-10-expressing T_H17 cell population compared with the control group (Figure 1D). Since IL-10-producing T_H17 cells have been described as restraining inflammation rather than promoting disease (McGeachy et al., 2007), we hypothesized that STING activation might redirect T_H17 cells to a less pathogenic phenotype.

STING expression and activity are inversely associated with T_H17 cell pathogenicity

Accumulating studies demonstrate that T_H17 cells are a heterogeneous subset with a spectrum of functional states ranging from non-pathogenic (or conventional) to a pathogenic phenotype (Stockinger and Omenetti, 2017). IL-6 and TGF-β are critical inducers of conventional T_H17 cells (cT_H17), which fail to promote tissue inflammation (Bettelli et al., 2006; McGeachy et al., 2007). On the other hand, although IL-23 does not stimulate T_H17 differentiation per se, it is crucial for inducing a pro-inflammatory pathogenic program in T_H17 cells (Langrish et al., 2005; McGeachy et al., 2009). The generation of T_H17 cells with a pathogenic profile (pT_H17) *in vitro* is obtained by activation with the cytokines IL-1β, IL-6, and IL-23 in a TGF-β-independent manner (Ghoreschi et al., 2010). We used both approaches to verify differential expression and activity of the STING pathway between cT_H17 and pT_H17 cells. We found that the *Tmem173* mRNA was intensely expressed after 48 h of culture in cT_H17 cells, declining at 72 h but still high compared with at 24 h. Contrariwise, pT_H17 only showed a slight and transient rise in *Tmem173* expression (Figure 2A). Accordingly, STING protein expression was more pronounced in cT_H17 than in pT_H17 cells (Figure 2B). Of note, IL-1β, IL-6, or IL-23 alone was insufficient to increase STING expression to that level observed in cT_H17 cells (Figure S1A), suggesting that the combination of IL-6 and TGF-β is the optimal signal required for STING expression in T_H17 cells.

We next evaluated the role of STING in both T_H17 cell profiles. As shown above, STING activation increased IL-10 production concomitantly with diminished expression of IL-17A (Figure 2C). These data were corroborated by the increase of *Il10* and reduction of *Il17a* and *Il23r* mRNA levels (Figure 2D), the latter being a key marker of T_H17 cell pathogenic phenotype (McGeachy et al., 2009). These effects were abolished in STING-deficient T cells (Figures 2C and 2D). Similarly, treatment with C-176, a potent and selective STING inhibitor (Haag et al., 2018), blocked the effect of agonist-induced STING activation on the T_H17 cell cytokine profile (Figure 2E). Also, C-176 blocked DMXAA effects on the mRNA expression of *Ifnb1*, *Il17a*, *Il23r*, *Il10*, and *Cd5l* (Figure 2F), the latter being a regulator of lipid metabolism linked with non-pathogenic T_H17 cells (Wang et al., 2015).

Additionally, we used cells from $STING^{Gt}$ mice that harbor a mutated inactive STING protein (Sauer et al., 2011) and found that $STING^{Gt}$ T_H17 cells phenocopied the cytokine profile found in STING-deficient T_H17 cells (Figure S1B). Interestingly, STING-deficient T_H17 cells showed even higher levels of IL-17A than wild-type (WT) cells, suggesting that STING is being activated during T cell activation *in vitro*. We speculated that nucleic acids released by T cells that die over the activation process or mitochondrial DNA released after cellular stress (Imanishi et al., 2014; West et al., 2015) might be potential endogenous ligands for STING activation in our setting, which merits further investigation.

STING-mediated IL-10 expression in T_H17 cells partially depends on aryl hydrocarbon receptor (AhR) signaling

STING-mediated IL-10 expression is essential for controlling colitis (Ahn et al., 2017). However, how STING induces IL-10 expression was still unaddressed. Once STING is activated, it triggers the production of IFNβ (Ishikawa and Barber, 2008). Moreover, it is known that IFNβ can upregulate IL-10 expression and reduce the inflammatory response elicited by T_H17 cells (Ramgolam et al., 2009; Zhang et al., 2011). We then asked whether STING restrains T_H17 pathogenicity by enhancing IFN-β-IFNAR signaling. Indeed, STING activation increased *Ifnb1* mRNA expression in cT_H17 cells (Figure 3A). However, DMXAA still promoted IL-17A decreased levels and enhanced IL-10 production in IFNAR-deficient T cells, indicating that STING regulates T_H17 cell pathogenicity through an IFNβ-IFNAR-independent mechanism (Figure 3B).

B lymphocyte-induced maturation protein 1 (Blimp-1), encoded by the *Prdm1* gene, is a transcriptional repressor that has been shown to promote IL-10 expression in T_H1 cells and T_H17 cells (Heinemann et al., 2014; Neumann et al., 2014). To investigate whether STING-mediated IL-10 production in T_H17 cells requires Blimp-1, we cultured WT or Blimp-1-deficient naive CD4 T cells (CD4-Cre $Prdm1^{fl/fl}$) under T_H17-skewing conditions with DMXAA. The absence of Blimp-1 did not affect the STING-driven IL-10 expression in T_H17 cells (Figure S2), ruling out a role of Blimp-1 in this process.

AhR is a ligand-activated transcriptional factor, activated by xenobiotic compounds and endogenous ligands, involved in T_H17 cell generation (Quintana et al., 2008; Veldhoen et al., 2008). Besides, AhR can also cooperate with cMaf to induce IL-10 production in T_R1 cells (Apetoh et al., 2010). We found that DMXAA did not affect *Maf* and *Ahr* gene expression in cT_H17 cells, but it increased *Cyp1a1* and *Ahrr* mRNA expression, which are transcriptional targets of AhR (Figure 3C), suggesting that STING activation triggers AhR transcriptional activity. Interestingly, STING and AhR expressions were higher in cT_H17 cells than in other CD4 T cell populations (Figure 3D). Furthermore, STING-deficient cT_H17 and pT_H17 cells showed reduced levels of AhR expression (Figure 3E). By analyzing a temporal expression of AhR protein levels after STING activation, we did not observe substantial differences until 72 h, when it was slightly decreased (Figure 3F), probably by degradation due to its increased activity (Davarinos and Pollenz, 1999). We, therefore, hypothesized that AhR might cooperate with STING signaling to induce a non-pathogenic program.

To test this hypothesis, we cultured cT_H17 in the presence of a STING agonist with or without CH223191, an AhR antagonist

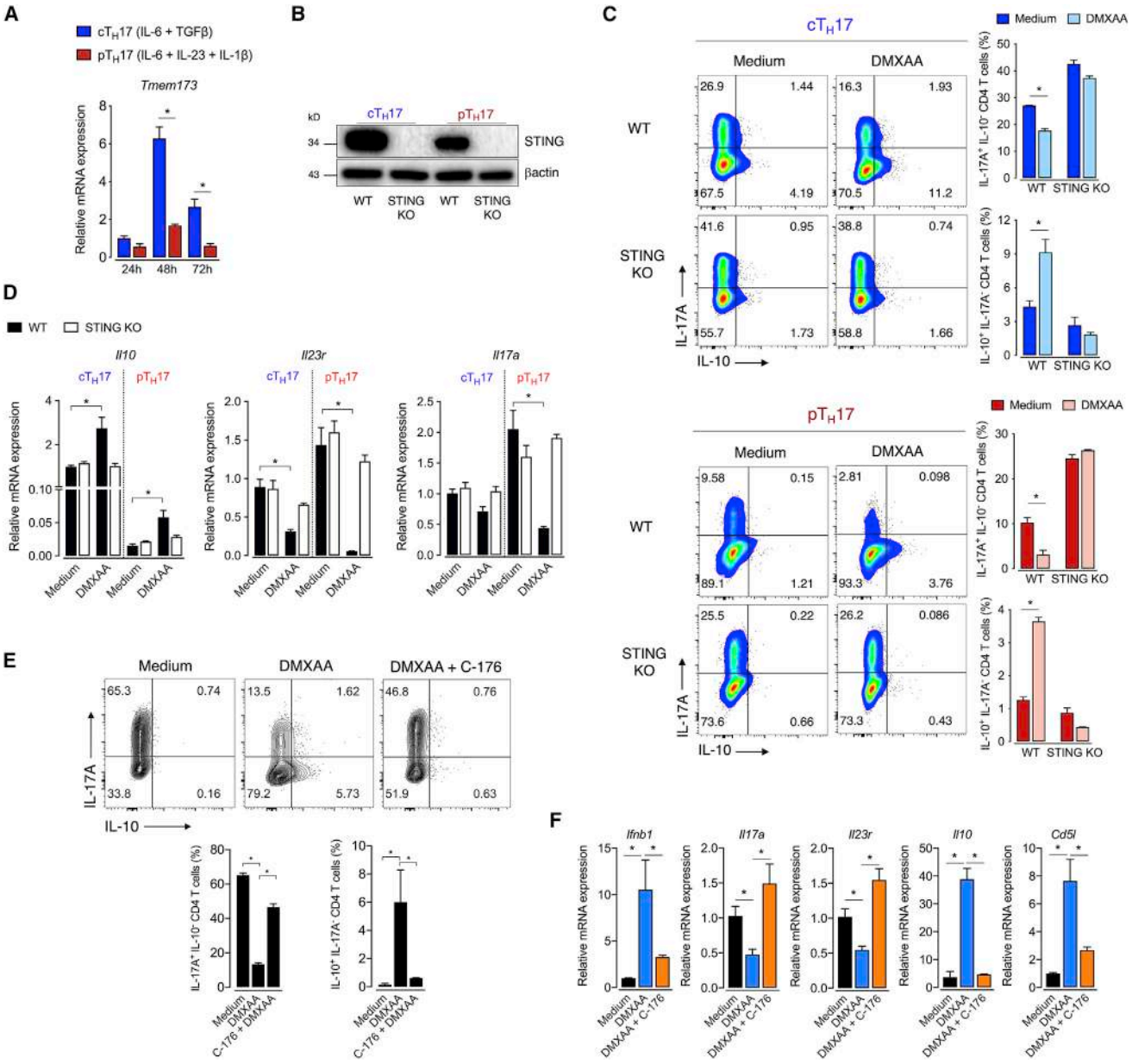

Figure 2. STING restrains the T_H17 cell pathogenic program

(A) Kinetic of *Tmem173* mRNA expression in cT_H17 and pT_H17 cells (n = 3). Fold change relative to cT_H17 at 24 h.

(B) STING protein expression in cT_H17 and pT_H17 cells at 72 h of culture. β-actin was used as the loading control.

(C) Flow-cytometric analysis of IL-10 and IL-17A expression in WT and STING-deficient cT_H17 and pT_H17 cells differentiated with DMXAA (10 μM) for 72 h (n = 3).

(D) *Il10*, *Il23r*, and *Il17a* mRNA expression in T_H17 cells cultured as in (C) at 48 h of culture. Fold change relative to cT_H17 WT control (medium).

(E) Flow-cytometric analysis of IL-10 and IL-17A expression in cT_H17 cell cultured with C-176 (1 μM) overnight followed by the addition of DMXAA for 72 h (n = 3).

(F) *Ifnb1*, *Il17a*, *Il23r*, *Il10*, and *Cd5l* mRNA expression in cT_H17 cells cultured as in (E) (n = 4). Fold change relative to control.

Data are representative of at least two independent experiments and are shown as mean ± SEM. *p < 0.05 determined by one-way ANOVA (E and F) or two-way ANOVA (A, C, and D) followed by Tukey's post hoc test.

See also Figure S1.

(Kim et al., 2006). Notably, AhR inhibition partially reduced the ability of DMXAA to increase IL-10 cytokine production (Figure 3G). Accordingly, AhR inhibition reduced STING-induced rise in the *Il10* mRNA levels and abrogation of *Il22* and *Cyp1a1*, both readouts of AhR signaling (Figure 3H). As previously reported (Veldhoen et al., 2009), AhR inhibition reduced T_H17 cell differentiation, and this effect was even augmented in the presence of DMXAA, as shown by the reduction of *Il17a* and *Il23r*

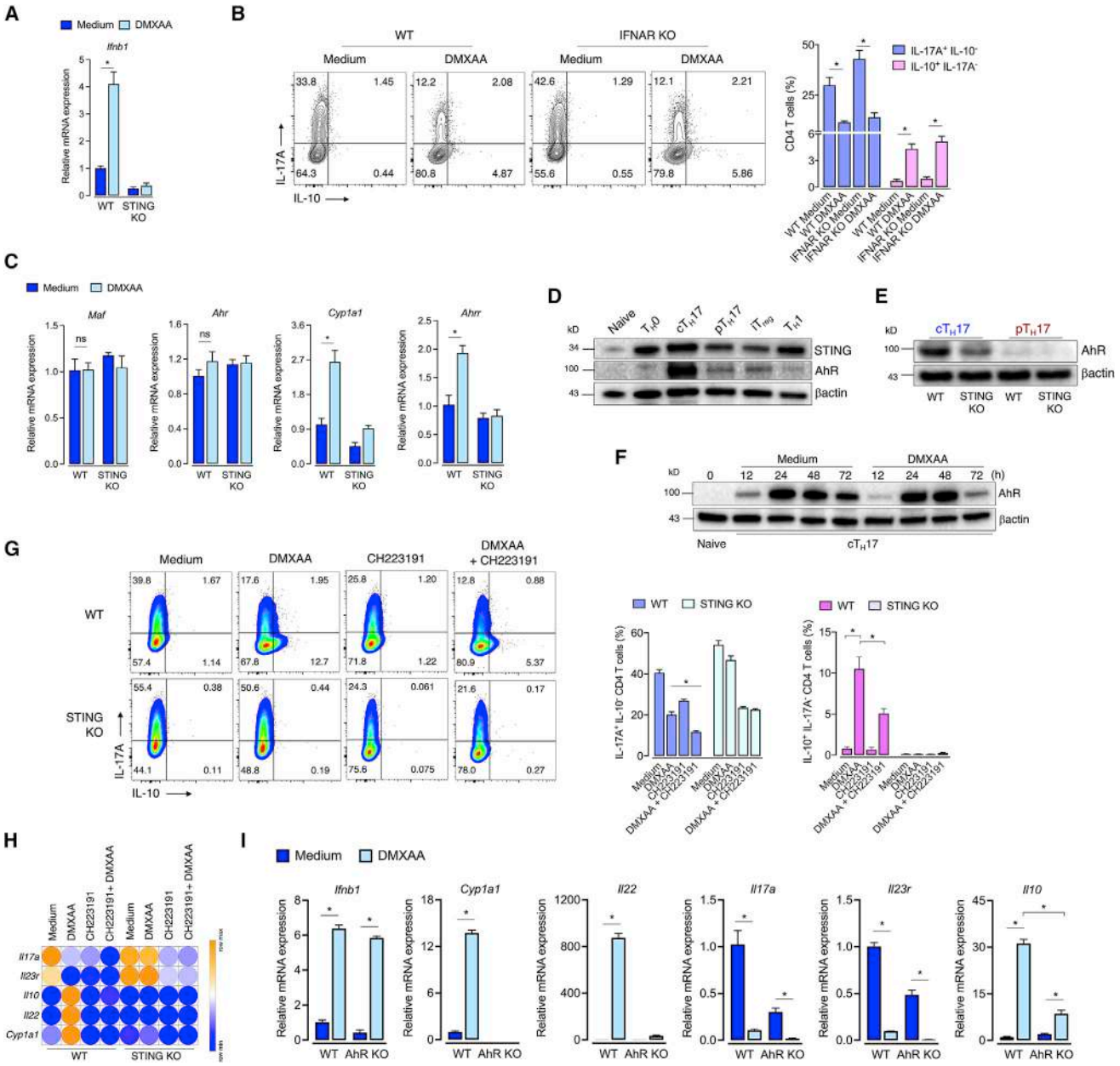

Figure 3. STING-mediated IL-10 expression in T_H17 cells is partially dependent on AhR

(A) *Ifnb1* mRNA expression in DMXAA-treated WT or STING-deficient cT_H17 cells at 48 h of culture (n = 3). Fold change relative to WT control.

(B) Flow cytometric analysis of IL-10 and IL-17A expression in WT or IFNAR-deficient cT_H17 cells cultured with DMXAA for 72 h (n = 3).

(C) *Maf*, *Ahr*, *Cyp1a1*, and *Ahrr* mRNA expression in DMXAA-treated WT or STING-deficient cT_H17 cells at 48 h of culture (n = 3). Fold change relative to WT control.

(D and E) STING and AhR protein expression in T_H subsets at 72 h of culture (left). AhR protein expression in WT and STING-deficient cT_H17 and pT_H17 cells (right). β-actin was used as the loading control.

(F) AhR protein expression in DMXAA-treated cT_H17 cells at different time points. β-actin was used as the loading control.

(G) Flow-cytometric analysis of IL-10 and IL-17A expression in WT and STING-deficient cT_H17 cells cultured with DMXAA and/or CH223191 (30 μM) for 72 h (n = 3).

(H) *Il17a*, *Il23r*, *Il10*, *Il22*, and *Cyp1a1* mRNA expression in cT_H17 cells cultured as in (G) (n = 4). Fold change relative to WT control. Data are displayed in a heatmap.

(I) *Ifnb1*, *Cyp1a1*, *Il22*, *Il17a*, *Il23r*, and *Il10* mRNA expression in WT and AhR-deficient cT_H17 cells cultured with DMXAA for 72 h (n = 4). Fold change relative to WT control.

Data are representative of at least two independent experiments and are shown as mean ± SEM. *$p < 0.05$ determined by two-way ANOVA (A–C, G, and I) followed by Tukey's post hoc test.

See also Figures S2 and S3.

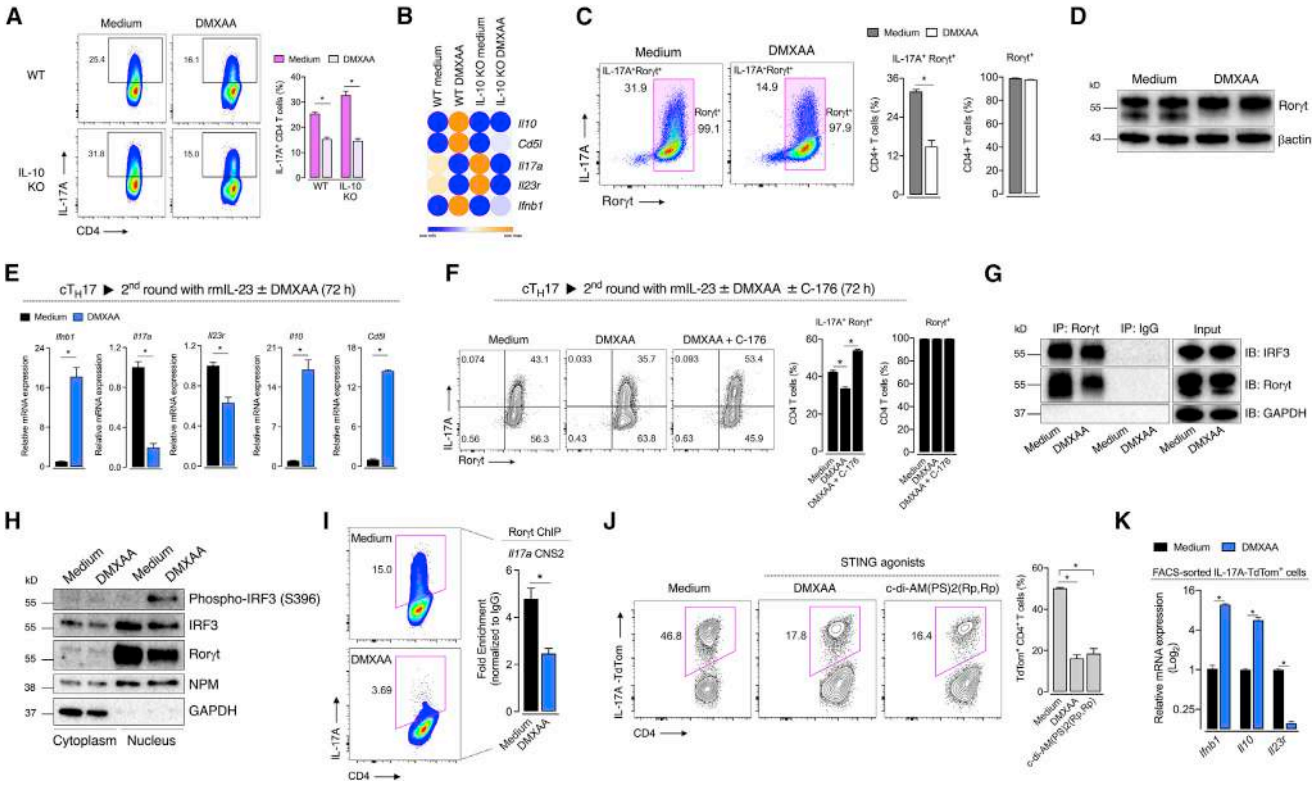

Figure 4. STING activation limits IL-17A expression through regulation of Rorγt transcriptional activity

(A) Flow-cytometric analysis of WT and IL-10-deficient cT$_H$17 cells cultured with DMXAA for 72 h (n = 4).

(B) *Il10*, *Cd5l*, *Il17a*, *Il23r*, and *Ifnb1* mRNA expression in cT$_H$17 cultured as in (A) (n = 3). Fold change relative to WT control. Data are displayed in a heatmap.

(C and D) Rorγt protein expression in cT$_H$17 cells cultured with DMXAA for 72 h as determined by flow cytometry (left; n = 4) and immunoblot (right). β-actin was used as the loading control.

(E) *Ifnb1*, *Il17a*, *Il23r*, *Il10*, and *Cd5l* mRNA expression in T$_H$17 cells after a second round of culture with rmIL-23 and DMXAA for 72 h (n = 4). Fold change relative to control.

(F) Flow-cytometric analysis of IL-17A and Rorγt expression in T$_H$17 cells cultured as in (E) with C-176 for 72 h (n = 5).

(G) Immunoprecipitation of Rorγt and IRF3. Control and DMXAA-treated cT$_H$17 cell lysates were subjected to IP with anti-Rorγt or immunoglobulin G (IgG) control, and immunoblot was performed as indicated. GAPDH was used as the input loading control.

(H) Immunoblot analysis of phospho-IRF3, IRF3, and Rorγt in cytoplasmic and nuclear fractions from control and DMXAA-treated cT$_H$17 cells. GAPDH and nucleophosmin (NPM) were used as the cytoplasmic and nuclear loading control, respectively.

(I) ChIP-qPCR analysis of Rorγt binding to the *Il17a* CNS2 enhancer region in control and DMXAA-treated cT$_H$17 for 72 h (n = 3). Data are depicted as fold enrichment to isotype IgG control.

(J) Flow-cytometric analysis of IL-17A-TdTom$^+$ cT$_H$17 cells cultured with DMXAA or c-di-AM(PS)2(Rp,Rp) (15 μM) for 72 h (n = 3).

(K) *Ifnb1*, *Il10*, and *Il23r* mRNA expression in sorted DMXAA-treated IL-17A-TdTom$^+$ cT$_H$17 cells at 72 h of culture (n = 4). Fold change relative to control.

Data are representative of at least two independent experiments and are shown as mean ± SEM. *p < 0.05 determined by two-tailed Student's t test (C, E, and I), one-way ANOVA (F and J), or two-way ANOVA (A and K) followed by Tukey's post hoc test.

See also Figure S4.

mRNA expression (Figures 3G and 3H). We confirmed these findings using STING-activated AhR-deficient cT$_H$17 cells, in which mRNA levels for *Cyp1a1*, *Il22*, *Il17a*, *Il23r*, and *Il10* phenocopied the pharmacological blockade of AhR (Figure 3I). Of note, AhR deficiency did not affect the DMXAA-induced *Ifnb1* mRNA expression (Figure 3I). On the other hand, in T$_H$1 cells, which barely express AhR (Quintana et al., 2008; Veldhoen et al., 2008), DMXAA did not affect IL-10 expression, although it slightly reduced the frequency of IFNγ-expressing T$_H$1 cells (Figure S3). Collectively, these data indicate that IL-10 production induced by activation of STING in T$_H$17 cells is partially dependent on AhR.

STING activation reduces Rorγt-mediated *Il17a* transcription

Since exogenous IL-10 inhibits T$_H$17 cell inflammatory functions (Huber et al., 2011; Zhang et al., 2011), we hypothesized that IL-10 produced by T$_H$17 cells upon STING activation would affect the IL-17A expression in an autocrine/paracrine manner. However, the reduction of IL-17A expression by DMXAA was maintained in IL-10-lacking T$_H$17 cells (Figure 4A). Moreover, activation of STING still induced downregulation of *Il17a* and *Il23r* mRNA in IL-10-deficient cells (Figure 4B). Thus, STING regulates pathogenicity of T$_H$17 cells independent of an IL-10-induced suppressive environment.

T_H17 cell differentiation and function require the activity of Rorγt, a transcriptional factor responsible for the expression of lineage signature genes such as *Il17a* and *Il23r* (Ivanov et al., 2006; Yang et al., 2008). We found that despite the STING activation causing a reduction in IL-17A production, it did not affect the expression of Rorγt (Figures 4C and 4D). Furthermore, when we exposed fully differentiated cT_H17 cells (100% of Rorγt$^+$ T cells) to IL-23 in the second round of culture, DMXAA still decreased *Il17a* and *Il23r* mRNA levels while augmenting the expression of *Il10* and *Cd5l* mRNAs (Figure 4E). Of interest, the treatment of cell cultures with STING inhibitor (C-176) along with the agonist in the second round of culture was sufficient to revert IL-17A levels (Figure 4F). Together, these data suggest that STING activation might reduce Rorγt transcriptional activity rather than its expression during T_H17 cell differentiation.

The canonical STING signaling cascade culminates in IRF3 phosphorylation and its subsequent translocation into the nucleus, triggering IFNβ production (Tanaka and Chen, 2012). STING activation induced the phosphorylation of IRF3 in cT_H17 cells (Figure 1C), but IFNAR signaling was dispensable for STING-induced IL-17A reduction (Figure 3B). Of note, it was reported that IRF3 restrains IL-17A expression in CD8 T cells through direct interaction with Rorγt, hampering its recruitment to the conserved noncoding sequence 2 (CNS2) enhancer region in the *Il17a* locus (De Lendonck et al., 2013). In fact, the binding of Rorγt on the CNS2 enhancer region of the *Il17a* locus plays an indispensable role in initiating *Il17a* transcription (Wang et al., 2012). Hence, we postulated that STING-driven activation of IRF3 could be a mechanism by which STING activation reduces the *Il17a* expression in T_H17 cells. Accordingly, we observed that IRF3 forms a complex with Rorγt in cT_H17 cells by immunoprecipitation analysis, but STING activation did not change the extent of this physical interaction (Figure 4G). Upon activation, IRF3 undergoes dimerization and phosphorylation, which is essential to form complexes with coactivators CBP/p300 in the nucleus and enable the transcription of its target genes (Chen et al., 2008). We found that DMXAA increased the expression of phosphorylated IRF3 almost exclusively in the nucleus of cT_H17 cells, which coincides with the high levels of Rorγt in the same compartment (Figure 4H). Importantly, the phosphorylation of IRF3 was abrogated in STING-deficient cells (Figure S4).

To confirm whether STING activation affects Rorγt transcriptional function, we performed the chromatin immunoprecipitation (ChIP) assay and analyzed the recruitment of Rorγt to the *Il17a* CNS2 enhancer region. Remarkably, DMXAA reduced the ability of Rorγt to bind to the CNS2 region (Figure 4I). As supported by a previous study (De Lendonck et al., 2013), it likely occurs via STING downstream activation of IRF3. Of note, we noticed basal levels of inactive IRF3 in the nuclear compartment of cT_H17 cells (Figures 4H and S4). This is consistent with studies showing that, before its activation, IRF3 is primarily found in the cytoplasm in a monomeric autoinhibitory state, and it can shuttle between cytoplasm and nucleus due to its constitutive active nuclear localization and nuclear-export signals. Nevertheless, only the phosphorylated dimeric form of IRF3 can induce transcriptional activity (Kumar et al., 2000; Zhu et al., 2015). Thus, it is likely that only the phosphorylated nuclear IRF3 is required to inhibit Rorγt-driven *Il17a* transcription after STING activation.

Finally, by crossing *Il17a*-Cre mice (Hirota et al., 2011) with TdTomato conditional reporter mice (Madisen et al., 2010), we generated a system in which TdTomato fluorescence emission only occurs whether the cell activates the *Il17a* transcription program (TdTom$^+$), reflecting transcriptional activity on *Il17a* locus. We observed that STING agonists reduced the frequency of IL-17A-TdTom$^+$ T cells compared with control, indicating that STING downstream signaling reduces *Il17a* transcription (Figure 4J). We also sorted IL-17A-TdTom$^+$ cells from T_H17 cultures and found that STING activation reduced *Il23r* mRNA levels while increasing the expression of *Il10* (Figure 4K).

STING signaling in undifferentiated T cells can cause antiproliferative and pro-apoptotic effects (Cerboni et al., 2017; Gulen et al., 2017; Larkin et al., 2017). In this context, apart from the TCR signal, the cytokine milieu has crucial implications over the transcriptional program that governs T cell survival and functions. For instance, IL-6 has been described to rescue T cells from death (Ayroldi et al., 1998). Thus, the apoptotic effect of STING signaling might be counterbalanced by pro-surviving signals of cytokines in T cells undergoing differentiation, especially in a disease setting. In this realm, we revealed here an intrinsic role of STING in restraining the T_H17 cell pathogenic program. We demonstrated that STING activation induced the production of IL-10 in T_H17 cells, decreasing IL-17A expression in a type I IFN-independent manner. This effect occurred partially through AhR-dependent signaling for the production of IL-10 along with IRF3-mediated reduction of Rorγt transcriptional activity for IL-17A. However, we cannot exclude the involvement of additional mechanisms. For instance, STING can also activate the nuclear factor κB (NF-κB) signaling pathway (Abe and Barber, 2014), which is considered an important transcriptional factor for IL-10 production in macrophages (Saraiva et al., 2005). Whether STING activation could regulate IL-10 expression via NF-κB activation remains to be determined.

STING has gained attention due to the complex and diverse biological functions it can exert upon activation by cytosolic double-stranded DNA (dsDNA) or cyclic dinucleotides (Li et al., 2017). Besides, recent reports show that some transmembrane carriers can enable an intercellular shuttle of cyclic dinucleotides into immune cells (Concepcion et al., 2022; Luteijn et al., 2019; Ritchie et al., 2019). Thus, it is reasonable to consider that cyclic dinucleotides released from host cells or even self-DNA from damaged tissue might activate STING in T_H17 cells, reprogramming their responses to a non-pathogenic profile as a mechanism to counteract chronic and autoimmune inflammation. In support of that, STING deficiency results in increased T_H17 cell tissue infiltration in a model of chronic pancreatitis (Zhao et al., 2019).

Limitations of the study

Our data imply that STING activation restrains the T_H17 pathogenic state. However, the major limitation of the current study is that we have not explored the T_H17-cell-intrinsic regulatory role of STING in a disease setting. Future *in vivo* experiments using appropriate conditional knockout mice and animal models are needed to confirm the extent and relevance of our findings in an inflammatory process. Another caveat is that we could not clarify how STING activates AhR signaling to induce IL-10 production in T_H17 cells, which merits further investigation.

STAR★METHODS

Detailed methods are provided in the online version of this paper and include the following:

- KEY RESOURCES TABLE
- RESOURCE AVAILABILITY
  - Lead contact
  - Materials availability
  - Data and code availability
- EXPERIMENTAL MODEL AND SUBJECT DETAILS
  - Mice
- METHOD DETAILS
  - *In vitro* T cell differentiation
  - RNA extraction and quantitative real-time PCR
  - Chromatin immunoprecipitation (ChIP)
  - Flow cytometry
  - Immunoblot and immunoprecipitation analysis
- QUANTIFICATION AND STATISTICAL ANALYSIS

SUPPLEMENTAL INFORMATION

Supplemental information can be found online at https://doi.org/10.1016/j.celrep.2022.110838.

ACKNOWLEDGMENTS

We thank all members of the Laboratory of Inflammation and Pain at Ribeirao Preto Medical School for technical support. This work was supported by a São Paulo Research Foundation (FAPESP) grant (no.13/08216-2 - Center for Research in Inflammatory Diseases), a National Council for Scientific and Technological Development (CNPq) grant (nos. 430823/2018-5 and 315880/2021-0), and a National Institutes of Health (NIH) grant (no. R01 AI116453). This work was also supported by FAPESP fellowships to L.E.A.D. (no. 18/17542-4), G.C.M.C. (no. 19/15070-0), and G.A.P. (no.20/04170-1).

AUTHOR CONTRIBUTIONS

L.E.A.D., F.Q.C., T.M.C., S.C.O., M.A.R.V., T.S., and J.C.A.-F. designed experiments and provided conceptual input. L.E.A.D., G.C.M.C., M.F.F., D.C.N., and G.A.P performed experiments. L.E.A.D. and J.C.A.-F. analyzed data and wrote the manuscript.

DECLARATION OF INTERESTS

All authors declare no competing interests.

Received: June 22, 2021
Revised: March 2, 2022
Accepted: April 28, 2022
Published: May 24, 2022

REFERENCES

Abe, T., and Barber, G.N. (2014). Cytosolic-DNA-mediated, STING-dependent proinflammatory gene induction necessitates canonical NF-κB activation through TBK1. J. Virol. *88*, 5328–5341. https://doi.org/10.1128/jvi.00037-14.

Abe, T., Harashima, A., Xia, T., Konno, H., Konno, K., Morales, A., Ahn, J., Gutman, D., and Barber, G.N. (2013). STING recognition of cytoplasmic DNA instigates cellular defense. Mol. Cell *50*, 5–15. https://doi.org/10.1016/j.molcel.2013.01.039.

Ahn, J., Son, S., Oliveira, S.C., and Barber, G.N. (2017). STING-dependent signaling underlies IL-10 controlled inflammatory colitis. Cell Rep. *21*, 3873–3884. https://doi.org/10.1016/j.celrep.2017.11.101.

Apetoh, L., Quintana, F.J., Pot, C., Joller, N., Xiao, S., Kumar, D., Burns, E.J., Sherr, D.H., Weiner, H.L., and Kuchroo, V.K. (2010). The aryl hydrocarbon receptor interacts with c-Maf to promote the differentiation of type 1 regulatory T cells induced by IL-27. Nat. Immunol. *11*, 854–861. https://doi.org/10.1038/ni.1912.

Ayroldi, E., Zollo, O., Cannarile, L., D' Adamio, F., Grohmann, U., Delfino, D.V., and Riccardi, C. (1998). Interleukin-6 (IL-6) prevents activation-induced cell death: IL-2–Independent inhibition of fas/fasL expression and cell death. Blood *92*, 4212–4219. https://doi.org/10.1182/blood.v92.11.4212.423k42_4212_4219.

Bettelli, E., Carrier, Y., Gao, W., Korn, T., Strom, T.B., Oukka, M., Weiner, H.L., and Kuchroo, V.K. (2006). Reciprocal developmental pathways for the generation of pathogenic effector TH17 and regulatory T cells. Nature *441*, 235–238. https://doi.org/10.1038/nature04753.

Burdette, D.L., Monroe, K.M., Sotelo-Troha, K., Iwig, J.S., Eckert, B., Hyodo, M., Hayakawa, Y., and Vance, R.E. (2011). STING is a direct innate immune sensor of cyclic di-GMP. Nature *478*, 515–518. https://doi.org/10.1038/nature10429.

Canesso, M.C.C., Lemos, L., Neves, T.C., Marim, F.M., Castro, T.B.R., Veloso, É., Queiroz, C.P., Ahn, J., Santiago, H.C., Martins, F.S., et al. (2018). The cytosolic sensor STING is required for intestinal homeostasis and control of inflammation. Mucosal Immunol. *11*, 820–834. https://doi.org/10.1038/mi.2017.88.

Cerboni, S., Jeremiah, N., Gentili, M., Gehrmann, U., Conrad, C., Stolzenberg, M.-C., Picard, C., Neven, B., Fischer, A., Amigorena, S., et al. (2017). Intrinsic antiproliferative activity of the innate sensor STING in T lymphocytes. J. Exp. Med. *214*, 1769–1785. https://doi.org/10.1084/jem.20161674.

Chang, J.T., Wherry, E.J., and Goldrath, A.W. (2014). Molecular regulation of effector and memory T cell differentiation. Nat. Immunol. *15*, 1104–1115. https://doi.org/10.1038/ni.3031.

Chen, W., Srinath, H., Lam, S.S., Schiffer, C.A., Royer, W.E., and Lin, K. (2008). Contribution of Ser386 and Ser396 to activation of interferon regulatory factor 3. J. Mol. Biol. *379*, 251–260. https://doi.org/10.1016/j.jmb.2008.03.050.

Concepcion, A.R., Wagner, L.E., Zhu, J., Tao, A.Y., Yang, J., Khodadadi-Jamayran, A., Wang, Y.-H., Liu, M., Rose, R.E., Jones, D.R., et al. (2022). The volume-regulated anion channel LRRC8C suppresses T cell function by regulating cyclic dinucleotide transport and STING–p53 signaling. Nat. Immunol. *23*, 287–302. https://doi.org/10.1038/s41590-021-01105-x.

Davarinos, N.A., and Pollenz, R.S. (1999). Aryl hydrocarbon receptor imported into the nucleus following ligand binding is rapidly degraded via the cytosplasmic proteasome following nuclear export. J. Biol. Chem. *274*, 28708–28715. https://doi.org/10.1074/jbc.274.40.28708.

Fernandez-Salguero, P., Pineau, T., Hilbert, D., McPhail, T., Lee, S.S.T., Lee, S., Kimura, S., Nebert, D.W., Nebert, D., Rudikoff, S., et al. (1995). Immune system impairment and hepatic fibrosis in mice lacking the dioxin-binding Ah receptor. Science *268*, 722–726. https://doi.org/10.1126/science.7732381.

Gagliani, N., Amezcua Vesely, M.C., Iseppon, A., Brockmann, L., Xu, H., Palm, N.W., De Zoete, M.R., Licona-Limón, P., Paiva, R.S., Ching, T., et al. (2015). Th17 cells transdifferentiate into regulatory T cells during resolution of inflammation. Nature *523*, 221–225. https://doi.org/10.1038/nature14452.

Ghoreschi, K., Laurence, A., Yang, X.-P., Tato, C.M., McGeachy, M.J., Konkel, J.E., Ramos, H.L., Wei, L., Davidson, T.S., Bouladoux, N., et al. (2010). Generation of pathogenic TH17 cells in the absence of TGF-β signalling. Nature *467*, 967–971. https://doi.org/10.1038/nature09447.

Gulen, M.F., Koch, U., Haag, S.M., Schuler, F., Apetoh, L., Villunger, A., Radtke, F., and Ablasser, A. (2017). Signalling strength determines proapoptotic functions of STING. Nat. Commun. *8*, 427. https://doi.org/10.1038/s41467-017-00573-w.

Haag, S.M., Gulen, M.F., Reymond, L., Gibelin, A., Abrami, L., Decout, A., Heymann, M., van der Goot, F.G., Turcatti, G., Behrendt, R., and Ablasser, A.

(2018). Targeting STING with covalent small-molecule inhibitors. Nature *559*, 269–273. https://doi.org/10.1038/s41586-018-0287-8.

Heinemann, C., Heink, S., Petermann, F., Vasanthakumar, A., Rothhammer, V., Doorduijn, E., Mitsdoerffer, M., Sie, C., Da Costa, O.P., Buch, T., et al. (2014). IL-27 and IL-12 oppose pro-inflammatory IL-23 in CD4+ T cells by inducing Blimp1. Nat. Commun. *5*, 3770. https://doi.org/10.1038/ncomms4770.

Hirota, K., Duarte, J.H., Veldhoen, M., Hornsby, E., Li, Y., Cua, D.J., Ahlfors, H., Wilhelm, C., Tolaini, M., Menzel, U., et al. (2011). Fate mapping of IL-17-producing T cells in inflammatory responses. Nat. Immunol. *12*, 255–263. https://doi.org/10.1038/ni.1993.

Huber, S., Gagliani, N., Esplugues, E., O'Connor, W., Huber, F.J., Chaudhry, A., Kamanaka, M., Kobayashi, Y., Booth, C.J., Rudensky, A.Y., et al. (2011). Th17 cells express interleukin-10 receptor and are controlled by Foxp3- and Foxp3+ regulatory CD4+ T cells in an interleukin-10-dependent manner. Immunity *34*, 554–565. https://doi.org/10.1016/j.immuni.2011.01.020.

Imanishi, T., Ishihara, C., Badr, M.E.S.G., Hashimoto-Tane, A., Kimura, Y., Kawai, T., Takeuchi, O., Ishii, K.J., Taniguchi, S., Noda, T., et al. (2014). Nucleic acid sensing by T cells initiates Th2 cell differentiation. Nat. Commun. *5*, 3566. https://doi.org/10.1038/ncomms4566.

Ishikawa, H., and Barber, G.N. (2008). STING is an endoplasmic reticulum adaptor that facilitates innate immune signalling. Nature *455*, 674–678. https://doi.org/10.1038/nature07317.

Ivanov, I.I., McKenzie, B.S., Zhou, L., Tadokoro, C.E., Lepelley, A., Lafaille, J.J., Cua, D.J., and Littman, D.R. (2006). The orphan nuclear receptor RORγt directs the differentiation program of proinflammatory IL-17+ T helper cells. Cell *126*, 1121–1133. https://doi.org/10.1016/j.cell.2006.07.035.

Kim, S.-H., Henry, E.C., Kim, D.-K., Kim, Y.H., Shin, K.J., Han, M.S., Lee, T.G., Kang, J.K., Gasiewicz, T.A., Ryu, S.H., and Suh, P.G. (2006). Novel compound 2-Methyl-2 H -pyrazole-3-carboxylic acid (2-methyl-4- o -tolylazo-phenyl)-amide (CH-223191) prevents 2,3,7,8-TCDD-induced toxicity by antagonizing the aryl hydrocarbon receptor. Mol. Pharmacol. *69*, 1871–1878. https://doi.org/10.1124/mol.105.021832.

Kumar, K.P., McBride, K.M., Weaver, B.K., Dingwall, C., and Reich, N.C. (2000). Regulated nuclear-cytoplasmic localization of interferon regulatory factor 3, a subunit of double-stranded RNA-activated factor 1. Mol. Cell. Biol. *20*, 4159–4168. https://doi.org/10.1128/mcb.20.11.4159-4168.2000.

Langrish, C.L., Chen, Y., Blumenschein, W.M., Mattson, J., Basham, B., Sedgwick, J.D., McClanahan, T., Kastelein, R.A., and Cua, D.J. (2005). IL-23 drives a pathogenic T cell population that induces autoimmune inflammation. J. Exp. Med. *201*, 233–240. https://doi.org/10.1084/jem.20041257.

Larkin, B., Ilyukha, V., Sorokin, M., Buzdin, A., Vannier, E., and Poltorak, A. (2017). Cutting edge: activation of STING in T cells induces type I IFN responses and cell death. J. Immunol. *199*, 397–402. https://doi.org/10.4049/jimmunol.1601999.

De Lendonck, L.Y., Tonon, S., Nguyen, M., Vandevenne, P., Welsby, I., Martinet, V., Molle, C., Charbonnier, L.M., Leo, O., and Goriely, S. (2013). Interferon regulatory factor 3 controls interleukin-17 expression in CD8 T lymphocytes. Proc. Natl. Acad. Sci. U S A *110*, E3189–E3197. https://doi.org/10.1073/pnas.1219221110.

Li, Y., Wilson, H.L., and Kiss-Toth, E. (2017). Regulating STING in health and disease. J. Inflamm. *14*, 11–21. https://doi.org/10.1186/s12950-017-0159-2.

Liu, S., Cai, X., Wu, J., Cong, Q., Chen, X., Li, T., Du, F., Ren, J., Wu, Y.-T., Grishin, N.V., and Chen, Z.J. (2015). Phosphorylation of innate immune adaptor proteins MAVS, STING, and TRIF induces IRF3 activation. Science *80*, 347. https://doi.org/10.1126/science.aaa2630.

Luteijn, R.D., Zaver, S.A., Gowen, B.G., Wyman, S.K., Garelis, N.E., Onia, L., McWhirter, S.M., Katibah, G.E., Corn, J.E., Woodward, J.J., and Raulet, D.H. (2019). SLC19A1 transports immunoreactive cyclic dinucleotides. Nature *573*, 434–438. https://doi.org/10.1038/s41586-019-1553-0.

Madisen, L., Zwingman, T.A., Sunkin, S.M., Oh, S.W., Zariwala, H.A., Gu, H., Ng, L.L., Palmiter, R.D., Hawrylycz, M.J., Jones, A.R., et al. (2010). A robust and high-throughput Cre reporting and characterization system for the whole mouse brain. Nat. Neurosci. *13*, 133–140. https://doi.org/10.1038/nn.2467.

McGeachy, M.J., Bak-Jensen, K.S., Chen, Y., Tato, C.M., Blumenschein, W., McClanahan, T., and Cua, D.J. (2007). TGF-β and IL-6 drive the production of IL-17 and IL-10 by T cells and restrain TH-17 cell-mediated pathology. Nat. Immunol. *8*, 1390–1397. https://doi.org/10.1038/ni1539.

McGeachy, M.J., Chen, Y., Tato, C.M., Laurence, A., Joyce-Shaikh, B., Blumenschein, W.M., McClanahan, T.K., O'Shea, J.J., and Cua, D.J. (2009). The interleukin 23 receptor is essential for the terminal differentiation of interleukin 17–producing effector T helper cells in vivo. Nat. Immunol. *10*, 314–324. https://doi.org/10.1038/ni.1698.

Motwani, M., Pesiridis, S., and Fitzgerald, K.A. (2019). DNA sensing by the cGAS–STING pathway in health and disease. Nat. Rev. Genet. *20*, 657–674. https://doi.org/10.1038/s41576-019-0151-1.

Neumann, C., Heinrich, F., Neumann, K., Junghans, V., Mashreghi, M.F., Ahlers, J., Janke, M., Rudolph, C., Mockel-Tenbrinck, N., Kühl, A.A., et al. (2014). Role of blimp-1 in programing th effector cells into IL-10 producers. J. Exp. Med. *211*, 1807–1819. https://doi.org/10.1084/jem.20131548.

Prantner, D., Perkins, D.J., Lai, W., Williams, M.S., Sharma, S., Fitzgerald, K.A., and Vogel, S.N. (2012). 5,6-Dimethylxanthenone-4-acetic acid (DMXAA) activates stimulator of interferon gene (STING)-dependent innate immune pathways and is regulated by mitochondrial membrane potential. J. Biol. Chem. *287*, 39776–39788. https://doi.org/10.1074/jbc.m112.382986.

Quintana, F.J., Basso, A.S., Iglesias, A.H., Korn, T., Farez, M.F., Bettelli, E., Caccamo, M., Oukka, M., and Weiner, H.L. (2008). Control of Treg and TH17 cell differentiation by the aryl hydrocarbon receptor. Nature *453*, 65–71. https://doi.org/10.1038/nature06880.

Ramgolam, V.S., Sha, Y., Jin, J., Zhang, X., and Markovic-Plese, S. (2009). IFN-β inhibits Human Th17 cell differentiation. J. Immunol. *183*, 5418–5427. https://doi.org/10.4049/jimmunol.0803227.

Ritchie, C., Cordova, A.F., Hess, G.T., Bassik, M.C., and Li, L. (2019). SLC19A1 is an importer of the immunotransmitter cGAMP. Mol. Cell *75*, 372–381.e5. https://doi.org/10.1016/j.molcel.2019.05.006.

Saraiva, M., Christensen, J.R., Tsytsykova, A.V., Goldfeld, A.E., Ley, S.C., Kioussis, D., and O'Garra, A. (2005). Identification of a macrophage-specific chromatin signature in the IL-10 locus. J. Immunol. *175*, 1041–1046. https://doi.org/10.4049/jimmunol.175.2.1041.

Sauer, J.D., Sotelo-Troha, K., Von Moltke, J., Monroe, K.M., Rae, C.S., Brubaker, S.W., Hyodo, M., Hayakawa, Y., Woodward, J.J., Portnoy, D.A., and Vance, R.E. (2011). The N-ethyl-N-nitrosourea-induced Goldenticket mouse mutant reveals an essential function of sting in the in vivo interferon response to Listeria monocytogenes and cyclic dinucleotides. Infect. Immun. *79*, 688–694. https://doi.org/10.1128/iai.00999-10.

Stockinger, B., and Omenetti, S. (2017). The dichotomous nature of T helper 17 cells. Nat. Rev. Immunol. *17*, 535–544. https://doi.org/10.1038/nri.2017.50.

Sun, L., Wu, J., Du, F., Chen, X., and Chen, Z.J. (2013). Cyclic GMP-AMP synthase is a cytosolic DNA sensor that activates the type I interferon pathway. Science *339*, 786–791. https://doi.org/10.1126/science.1232458.

Tan, X., Sun, L., Chen, J., and Chen, Z.J. (2018). Detection of microbial infections through innate immune sensing of nucleic acids. Annu. Rev. Microbiol. *72*, 447–478. https://doi.org/10.1146/annurev-micro-102215-095605.

Tanaka, Y., and Chen, Z.J. (2012). STING specifies IRF3 phosphorylation by TBK1 in the cytosolic DNA signaling pathway. Sci. Signal. *5*, ra20. https://doi.org/10.1126/scisignal.2002521.

Veldhoen, M., Hirota, K., Westendorf, A.M., Buer, J., Dumoutier, L., Renauld, J.C., and Stockinger, B. (2008). The aryl hydrocarbon receptor links TH17-cell-mediated autoimmunity to environmental toxins. Nature *453*, 106–109. https://doi.org/10.1038/nature06881.

Veldhoen, M., Hirota, K., Christensen, J., O'Garra, A., and Stockinger, B. (2009). Natural agonists for aryl hydrocarbon receptor in culture medium are essential for optimal differentiation of Th17 T cells. J. Exp. Med. *206*, 43–49. https://doi.org/10.1084/jem.20081438.

Wang, C., Yosef, N., Gaublomme, J., Wu, C., Lee, Y., Clish, C.B., Kaminski, J., Xiao, S., Zu Horste, G.M., Pawlak, M., et al. (2015). CD5L/AIM regulates lipid biosynthesis and restrains Th17 cell pathogenicity. Cell *163*, 1413–1427. https://doi.org/10.1016/j.cell.2015.10.068.

Wang, X., Zhang, Y., Yang, X.O., Nurieva, R.I., Chang, S.H., Ojeda, S.S., Kang, H.S., Schluns, K.S., Gui, J., Jetten, A.M., and Dong, C. (2012). Transcription of Il17 and Il17f is controlled by conserved noncoding sequence 2. Immunity *36*, 23–31. https://doi.org/10.1016/j.immuni.2011.10.019.

West, P., Khoury-Hanold, W., Staron, M., Tal, M.C., Pineda, C.M., Lang, S.M., Bestwick, M., Duguay, B.A., Raimundo, N., MacDuff, D.A., et al. (2015). Mitochondrial DNA stress primes the antiviral innate immune response. Nature *520*, 553–557. https://doi.org/10.1016/j.bpj.2014.11.029.

Yang, X.O., Pappu, B.P., Nurieva, R., Akimzhanov, A., Kang, H.S., Chung, Y., Ma, L., Shah, B., Panopoulos, A.D., Schluns, K.S., et al. (2008). T helper 17 lineage differentiation is programmed by orphan nuclear receptors RORα and RORγ. Immunity *28*, 29–39. https://doi.org/10.1016/j.immuni.2007.11.016.

Zhang, C., Shang, G., Gui, X., Zhang, X., Bai, X., and Chen, Z.J. (2019). Structural basis of STING binding with and phosphorylation by TBK1. Nature *567*, 394–398. https://doi.org/10.1038/s41586-019-1000-2.

Zhang, L., Yuan, S., Cheng, G., and Guo, B. (2011). Type I IFN promotes IL-10 production from T cells to suppress Th17 cells and Th17-associated autoimmune inflammation. PLoS One *6*, e28432. https://doi.org/10.1371/journal.pone.0028432.

Zhao, Q., Manohar, M., Wei, Y., Pandol, S.J., and Habtezion, A. (2019). STING signalling protects against chronic pancreatitis by modulating Th17 response. Gut *68*, 1827–1837. https://doi.org/10.1136/gutjnl-2018-317098.

Zhong, B., Yang, Y., Li, S., Wang, Y.Y., Li, Y., Diao, F., Lei, C., He, X., Zhang, L., Tien, P., and Shu, H.B. (2008). The adaptor protein MITA links virus-sensing receptors to IRF3 transcription factor Activation. Immunity *29*, 538–550. https://doi.org/10.1016/j.immuni.2008.09.003.

Zhu, M., Fang, T., Li, S., Meng, K., and Guo, D. (2015). Bipartite nuclear localization signal controls nuclear import and DNA-binding activity of IFN regulatory factor 3. J. Immunol. *195*, 289–297. https://doi.org/10.4049/jimmunol.1500232.

STAR★METHODS

KEY RESOURCES TABLE

REAGENT or RESOURCE	SOURCE	IDENTIFIER
Antibodies		
NA/LE Hamster Anti-Mouse CD3ε (clone 145-2C11)	BD Biosciences	Cat# 553057; RRID:AB_394590
NA/LE Hamster Anti-Mouse CD28 (clone 37.51)	BD Biosciences	Cat# 553294; RRID:AB_394763
Rat Anti-Mouse CD4-FITC (clone RM4-5)	BD Biosciences	Cat# 553047; RRID:AB_394583
Rat Anti-Mouse CD4-PerCP-Cy5.5 (clone RM4-5)	BD Biosciences	Cat# 550954; RRID:AB_393977
Rat Anti-Mouse CD4-APC (clone RM4-5)	BD Biosciences	Cat# 553051; RRID:AB_398528
Rat Anti-Mouse CD44-APC (clone IM7)	BD Biosciences	Cat# 559250; RRID:AB_398661
Rat Anti-Mouse CD62L-PE (clone MEL-14)	BD Biosciences	Cat# 553151; RRID:AB_394666
Rat Anti-Mouse IL17A-BV421 (clone TC11-18H10)	BD Biosciences	Cat# 563354; RRID:AB_2687547
Rat Anti-Mouse IL-17A-PE (clone TC11-18H10)	BD Biosciences	Cat# 559502; RRID:AB_397256
Rat Anti-Mouse IL-17A-APC (clone TC11-18H10)	BD Biosciences	Cat# 560184; RRID:AB_1645204
Rat Anti-Mouse IL-10-APC (clone JES5-16E3)	BD Biosciences	Cat# 554468; RRID:AB_398558
Rat Anti-Mouse IL-10-BV421 (clone JES5-16E3)	BD Biosciences	Cat# 563276; RRID:AB_2738111
Mouse Anti-Mouse Rorγt-AF647 (clone Q31-378)	BD Biosciences	Cat# 562682; RRID:AB_2687546
Mouse Anti-Mouse Rorγt-PerCP-Cy5.5 (clone Q31-378)	BD Biosciences	Cat# 562683; RRID:AB_2737720
Rat Anti-Mouse IL-10-PE (clone JES5-16E3)	eBioscience	Cat# 12-7101-82; RRID:AB_466176
Rat Anti-Mouse IFNγ-FITC (clone XMG1.2)	eBioscience	Cat# 11-7311-82; RRID:AB_465412
Rabbit Anti-Phospho-IRF3 (S396) (clone D6O1M)	Cell Signaling	Cat# 29047; RRID:AB_2773013
Rabbit Anti-IRF3 (clone D83B9)	Cell Signaling	Cat# 4302; RRID:AB_1904036
Rabbit Anti-Phospho-TBK1 (S172) (clone D52C2)	Cell Signaling	Cat# 5483; RRID:AB_10693472
Rabbit Anti-TBK1 (clone D1B4)	Cell Signaling	Cat# 3504; RRID:AB_2255663
Rabbit Anti-Phospho-STING (S365) (clone D8F4W)	Cell Signaling	Cat# 72971; RRID:AB_2799831
Rabbit Anti-STING (clone D2P2F)	Cell Signaling	Cat# 13647; RRID:AB_2732796
Rabbit Anti-AhR (polyclonal)	Enzo Life Sciences	Cat# BML-SA210; RRID:AB_10540536
Rabbit Anti-Rorγt (clone EPR20006)	Abcam	Cat# ab207082; RRID:AB_2889310
Anti-Rorγt (clone AFKJS-9)	Invitrogen	Cat# 14-6988-82; RRID:AB_1834475
Mouse Anti-GAPDH (clone D4C6R)	Cell Signaling	Cat# 97166; RRID:AB_2756824
Mouse Anti-βactin (clone 8H10D10)	Cell Signaling	Cat# 3700; RRID:AB_2242334
Rabbit Anti-NPM (polyclonal)	Cell Signaling	Cat# 3542; RRID:AB_2155178
Normal Rabbit IgG	Cell Signaling	Cat# 2729; RRID:AB_1031062
Goat Anti-rabbit IgG HRP	Sigma-Aldrich	Cat# A0545; RRID:AB_257896
Rabbit Anti-Mouse IgG HRP	Sigma-Aldrich	Cat# A9044; RRID:AB_258431
Biological samples		
HyClone™ Fetal Bovine Serum	GE Healthcare	Cat# SV30160.03
Chemicals, peptides, and recombinant proteins		
PBS (Phosphate buffered saline) 1X	Corning	Cat# 21-040
CD4 (L3T4) MicroBeads, mouse	Miltenyi Biotec	Cat# 130-117-043
Laemmli sample buffer	Bio-Rad	Cat# 161-0737
4–20% Mini-PROTEAN® TGX™ Precast Protein Gels	Bio-Rad	Cat# 4561094
Trans-Blot Turbo Mini Nitrocellulose Transfer Packs	Bio-Rad	Cat #1704158
β-Mercaptoethanol	Sigma-Aldrich	Cat# M6250
IMDM (Iscove's Modification of DMEM)	Corning	Cat# 15-016
L-Glutamine	Corning	Cat# 25-005
Penicillin-Streptomycin	Sigma-Aldrich	Cat# P4333

(*Continued on next page*)

Continued

REAGENT or RESOURCE	SOURCE	IDENTIFIER
Foxp3/Transcription Factor Staining Buffer Set	Invitrogen	Cat# 00-5523-00
Bovine serum albumin (BSA)	Sigma-Aldrich	Cat# A9418
β-Mercaptoethanol for cell culture	GIBCO	Cat# 21985023
Fixable Viability Dye eFluor™ 780	Invitrogen	Cat# 65-0865-14
Power SYBR Green Master Mix	Applied Biosystems	Cat# 4368708
iQ™ SYBR® Green Supermix	Bio-Rad	Cat# 1708886
PMA	Sigma-Aldrich	Cat# P1585
Ionomycin	Sigma-Aldrich	Cat# I0634
BD GolgiStop™ (containing Monensin)	BD Biosciences	Cat# 554724
Recombinant mIL-6	R&D Systems	Cat# 406-ML
Recombinant mIL-1β	R&D Systems	Cat# 401-ML
Recombinant mIL-23	R&D Systems	Cat# 1887-ML
Recombinat hTGF-β1	eBioscience	Cat# 14-8348-62
Recombinant mIL-12	R&D Systems	Cat# 419-ML
Recombinant mIL-2	R&D Systems	Cat# 402-ML
Protease/Phosphatase Inhibitor Cocktail (100X)	Cell Signaling	Cat# 5872
ECL Prime	GE Healthcare	Cat# RPN2236
DMXAA	Invivogen	Cat# tlrl-dmx
c-di-AMP	Invivogen	Cat# tlrl-nacda
c-di-GMP	Invivogen	Cat# tlrl-nacdg
2′3′-c-di-AM(PS)2 (Rp,Rp)	Invivogen	Cat# tlrl-nacda2r
C-176	Sigma-Aldrich	Cat# SML2559
CH223191	Tocris	Cat# 3858
Critical commercial assays		
RNA Isolation RNeasy Mini Kit	QIAGEN	Cat# 74104
Bicinchoninic Acid (BCA) kit for Protein Determination	Sigma-Aldrich	Cat# BCA1
Pierce™ Co-Immunoprecipitation Kit	Thermo Scientific	Cat# 26149
NE-PER Nuclear and Cytoplasmic Extraction Kit	Thermo Scientific	Cat# 78835
High-Capacity cDNA Reverse Transcription Kit	Applied Biosystems	Cat# 4368813
MAGnify™ Chromatin Immunoprecipitation System	Applied Biosystems	Cat# 492024
Experimental models: Organisms/strains		
Mouse: C57BL/6	The Jackson Laboratory	N/A
Mouse: IL-10 KO (B6.129P2-Il10tm1Cgn/J)	The Jackson Laboratory	Stock No: 002251
Mouse: IFNAR KO (B6(Cg)-Ifnar1tm1.2Ees/J)	The Jackson Laboratory	Stock No: 028288
Mouse: STING^{Gt} (C57BL/6J-Tmem173gt/J)	The Jackson Laboratory	Stock No: 017537
Mouse: *Il17a*-Cre (Il17atm1.1(icre)Stck/J)	The Jackson Laboratory	Stock No: 016879
Mouse: Ai14 (B6.Cg-Gt(ROSA)26Sortm14 (CAG-tdTomato)Hze/J)	The Jackson Laboratory	Stock No: 007914
Mouse: *Prdm1* floxed (B6.129-Prdm1tm1Clme/J)	The Jackson Laboratory	Stock No: 008100
Mouse: CD4-Cre Tg(Cd4-cre)1Cwi/BfluJ	The Jackson Laboratory	Stock No: 017336
Mouse: STING KO	Gift from Dr. Sergio C. Oliveira	(Ishikawa and Barber, 2008)
Mouse: AhR KO	Gift from Dr. Bernhard Ryffel	(Fernandez-Salguero et al., 1995)
Oligonucleotides		
Il23r fwd: 5′-GCCAAGAAGACCATTCCCGA-3′ *Il23r* rev: 5′-TCAGTGCTACAATCTTCTTCAGAGGACA-3′	Merck	N/A
Il17a fwd: 5′-GCTCCAGAAGGCCCTCAG-3′ *Il17a* rev: 5′-CTTTCCCTCCGCATTGACA-3′	Merck	N/A
Il22 fwd: 5′-CAGCTCCTGTCACATCAGCGGT-3′ *Il22* rev: 5′-AGGTCCAGTTCCCCAATCGCCT-3′	Merck	N/A

(*Continued on next page*)

Continued

REAGENT or RESOURCE	SOURCE	IDENTIFIER
Ifnb1 fwd: 5′-CAGCTCCAAGAAAGGACGAAC-3′ *Ifnb1* rev: 5′-GGCAGTGTAACTCTTCTGCAT-3′	Merck	N/A
Maf fwd: 5′-AGCAGTTGGTGACCATGTCG-3′ *Maf* rev: 5′-TGGAGATCTCCTGCTTGAGG-3′	Merck	N/A
Ahr fwd:5′-CAAATCAGAGACTGGCAGGA-3′ *Ahr* rev: 5′-AGAAGACCAAGGCATCTGCT-3′	Merck	N/A
Ahrr fwd: 5′-ACAGGGCAGACATTGTGGTT-3′ *Ahrr* rev: 5′-CCTGAGGCACAGACATGAAG-3′	Merck	N/A
Cd5l fwd: 5′-GAGGACACATGGATGGAATGT-3′ *Cd5l* rev: 5′-ACCCTTGTGTAGCACCTCCA-3′	Merck	N/A
Cyp1a1 fwd: 5′-GTTCTTGGAGCTTCCCCGAT-3′ *Cyp1a1* rev: 5′-CTGACACGAAGGCTGGAAGT-3′	Merck	N/A
Il10 fwd: 5′-ATAACTGCACCCACTTCCCA-3′ *Il10* rev: 5′-GGGCATCACTTCTACCAGGT-3′	Merck	N/A
Gapdh fwd: 5′-CATCTTCTTGTGCAGTGCCA-3′ *Gapdh* rev: 5′-CGGCCAAATCCGTTCAC-3′	Merck	N/A
Tmem173: IDT assay ID Mm.PT.58.7864131.g	IDT	N/A
Gapdh: IDT assay ID Mm.PT.39a.1	IDT	N/A
Il17a CNS2 (ChIP) fwd: 5′-CCGTTTAGACTTGAAACCCAGTC-3′ *Il17a* CNS2 (ChIP) rev: 5′-GTACCTATGTGTTAGGAGGCGC-3′	Eurofins Genomics	N/A
Software and algorithms		
FACSuite™ software	BD Biosciences	N/A
BD FACSDiva™ software	BD Biosciences	N/A
FlowJo™ v10	BD Biosciences	https://www.flowjo.com
StepOne Software v2.3	Applied Biosystems	N/A
Morpheus	Broad Institute	https://software.broadinstitute.org/morpheus/
Image Lab v6.1	Bio-Rad	https://www.bio-rad.com
Prism 8	GraphPad	https://www.graphpad.com

RESOURCE AVAILABILITY

Lead contact

Further information and requests for resources and reagents should be directed to and will be fulfilled by the lead contact, Jose C. Alves-Filho (jcafilho@usp.br).

Materials availability

This study did not generate new unique reagents.

Data and code availability

- Data reported in this paper will be shared by the lead contact upon request.
- This paper does not report original code.
- Any additional information required to reanalyze the data reported in this paper is available from the lead contact upon request.

EXPERIMENTAL MODEL AND SUBJECT DETAILS

Mice

C57BL/6 wild-type (WT), IL-10 KO (B6.129P2-Il10tm1Cgn/J), IFNAR KO (B6(Cg)-Ifnar1tm1.2Ees/J), STING^{Gt} (C57BL/6J-Tmem173gt/J), TdTomato reporter (Ai14; B6.Cg-Gt(ROSA)26Sortm14(CAG-tdTomato)Hze/J), *Il17a*-Cre (Il17atm1.1(icre)Stck/J), *Prdm1*-floxed (B6.129-Prdm1tm1Clme/J), CD4-Cre (Tg(Cd4-Cre)1Cwi/BfluJ) mice were obtained from Jackson Laboratories. STING KO mice (Ishikawa and Barber, 2008) were kindly provided by Dr. Sergio Costa Oliveira (Federal University of Minas Gerais, Brazil), and AhR KO mice (Fernandez-Salguero et al., 1995) were kindly provided by Dr. Bernhard Ryffel (CNRS Orleans, France).

All mice were maintained in specific-pathogen-free conditions at the Ribeirao Preto Medical School under controlled temperature (22–25°C), 12-h light-dark cycle, and provided with water and food *ad libitum*. Eight- to ten-week-old age- and sex-matched male and female mice were used for the experiments. All experiments were performed with permission from and in accordance with the Ethics Committee on Animal Use guidelines of Ribeirao Preto Medical School, University of Sao Paulo (protocol number 095/2019).

METHOD DETAILS

In vitro T cell differentiation

$CD4^+$ T cells were enriched from mice lymph nodes and spleen with anti-CD4 microbeads by using an AutoMACS magnetic cell sorter (Miltenyi Biotec) according to the manufacturer's protocol. Thereafter, naive $CD4^+CD62L^{high}CD44^{low}$ T cells were purified using a FACSAria III cell sorter (BD Biosciences). The sort-purified naive CD4 T cells were TCR-activated with plate-bound anti-CD3ε (4 μg/mL) and anti-CD28 (2 μg/mL) (BD Biosciences) in complete IMDM (supplemented with 10% FBS, L-glutamine, penicillin-streptomycin and β−mercaptoethanol). Skewing conditions were as follows: 1 ng/mL rhTGF-β1 (eBioscience) plus 25 ng/mL rmIL-6 (R&D Systems) for cT_H17; 25 ng/mL rmIL-6, 20 ng/mL rm-IL-1β and 30 ng/mL rmIL-23 (all from R&D Systems) for pT_H17; 1 ng/mL rhTGF-β1 for iT_{reg}; 20 ng/mL rmIL-12 and 20 ng/mL rmIL-2 (both from R&D Systems) for T_H1. When indicated, CH223191 (30 μM; Tocris), DMXAA (3–30 μM; Invivogen), C-176 (1 μM; Sigma-Aldrich), c-di-AM(PS)2 (Rp,Rp) (15 μM; Invivogen), c-di-AMP or c-di-GMP (both 30–100 μM; Invivogen) were used.

RNA extraction and quantitative real-time PCR

Total RNA from CD4 T cells was obtained using the RNeasy Isolation Kit according to the manufacturer's instructions (Qiagen). Total RNA was quantified, followed by conversion to cDNA using the High Capacity cDNA Reverse Transcription Kit (Applied Biosystems). Quantitative real-time PCR (qPCR) was performed with SYBR Green PCR Master Mix (Applied Biosystems) using a StepOnePlus Real-Time PCR machine (Applied Biosystems). Gene expression was determined relative to *Gapdh,* and fold change was calculated using the $2^{-\Delta\Delta CT}$ threshold cycle method. Heat maps were generated using the Morpheus web interface (https://software.broadinstitute.org/morpheus). Gene expression correlates with color intensity and data (replicates mean) were row-normalized. A list of primer pairs used for RT-qPCR is presented in the key resources table.

Chromatin immunoprecipitation (ChIP)

ChIP assays were performed with the MAGnify™ Chromatin Immunoprecipitation System (Life Technologies). Briefly, naive CD4 T cells were cultured under cT_H17-skewing conditions in the presence or absence of 10 μM DMXAA for 72 h. 4.5×10^6 cells were cross-linked with 1% formaldehyde for 10 min at room temperature and quenched with 0.125 M glycine. Samples were lysed and chromatin sheared using a Bioruptor Plus (Diagenode) sonication system to obtain 200- to 500-bp fragments (14 cycles, 30″ on, 30″ off, high setting). Chromatin-protein complexes were immunoprecipitated with either 5 μg anti-Rorγt (Invitrogen) or IgG control that were pre-bound to Protein A/G Dynabeads™ (Invitrogen) overnight on a rotator at 4°C. Afterward, cross-linking was reversed, and DNA was eluted and purified according to the supplier's instructions. Purified DNA was used for qPCR analysis with iQ™SYBR Green real-time PCR kit (Bio-Rad) using primers encompassing the *Il17a* CNS2 enhancer region, listed in the key resources table. Data were calculated ($2^{-(\Delta CT\ IP\ -\ \Delta CT\ control)}$) and presented as fold enrichment over IgG control.

Flow cytometry

For intracellular cytokine staining, T cells were stimulated for 4 h with phorbol 12-myristate 13-acetate (PMA) (50 ng/mL; Sigma-Aldrich) and ionomycin (500 ng/mL; Sigma-Aldrich) in the presence of a protein-transport inhibitor containing monensin (GolgiStop 1.5 μg/mL; BD Biosciences). For surface staining, cells were incubated with a fixable viability dye (Invitrogen) to exclude dead cells and fluorochrome-labeled monoclonal antibodies for the indicated markers. Thereafter, cells were fixed and permeabilized with the Foxp3 Fixation/Permeabilization Kit (Invitrogen), followed by intracellular staining. Data were acquired on FACSVerse or FACSCanto II machines (BD Biosciences) and analyzed using FlowJo software (BD Biosciences).

Immunoblot and immunoprecipitation analysis

Whole-cell lysates were obtained using RIPA lysis buffer (Sigma-Aldrich) containing protease and phosphatase inhibitor cocktail (Cell Signaling). Protein concentration was determined with the BCA protein assay (Sigma-Aldrich), and then cell lysates were mixed in Laemmli Sample Buffer (Bio-Rad) containing β−mercaptoethanol (95°C, 5 min). For separation by electrophoresis, 10 μg of total protein was loaded onto Mini-PROTEAN TGX Precast Protein Gel (Bio-Rad) and transferred to a nitrocellulose membrane using the Trans-Blot Turbo Transfer Pack (Bio-Rad). Membranes were treated with block buffer (5% non-fat milk in 0.1% TBS-Tween-20) at room temperature for 1 h and then probed overnight at 4°C with primary antibodies against STING (1:1000), IRF3 (1:1000), TBK1 (1:1000), phospho(S365)-STING (1:500), phospho(S396)-IRF3 (1:500), phospho(S172)-TBK1 (1:500) (all from Cell Signaling), AhR (1:3000; Enzo Life Sciences) or Rorγt (1:1000; Abcam). βactin or GAPDH (1:1000; Cell Signaling) served as loading controls. All primary antibodies were detected with appropriate HRP-conjugated secondary antibodies (Sigma-Aldrich; 1:5000). Detection was performed using ECL prime reagent (GE Healthcare) and chemiluminescence signals were recorded on the

ChemiDoc XRS+ imaging system (Bio-Rad). Data were analyzed with Image Lab (Bio-Rad). Cytoplasmic and nuclear fractionation was performed by using the NE-PER Extraction kit (Thermo Scientific) according to the manufacturer's recommendations. GAPDH and NPM (1:1000; Cell Signaling) were used as cytoplasmic and nuclear loading controls, respectively. Immunoprecipitation was performed using the Pierce co-IP kit (Thermo Scientific) following the manufacturer's protocol. Briefly, anti-Rorγt (Abcam) was immobilized using AminoLink Plus coupling resin. Equal amounts of cell lysates were precleared, followed by incubation with the antibody-coupled resin overnight at 4°C. The immunoprecipitate was eluted and subsequent immunoblot analysis was performed as described above.

QUANTIFICATION AND STATISTICAL ANALYSIS

Statistical analysis was performed using GraphPad Prism 8.0 software. Comparisons for two groups were calculated using unpaired two-tailed Student's t-tests. Multiple-group comparisons were performed with either one-way ANOVA or two-way ANOVA followed by Tukey's post hoc test. p value <0.05 was considered significant. Data are depicted as means $\pm$ SEM.